AgriEngineering

MDPI

Article

Stone Detection on Agricultural Land Using Thermal Imagery from Unmanned Aerial Systems

Florian Thürkow [1,2,*], Mike Teucher [3], Detlef Thürkow [4] and Milena Mohri [2]

[1] Institute for Geo-Information and Land Surveying, Anhalt University of Applied Sciences, Seminarplatz 2a, 06846 Dessau, Germany
[2] Umwelt-und Geodaten Management GbR, 06108 Halle (Saale), Germany; mohri@umgeodat.de
[3] Department of Geoecology, Institute of Geosciences and Geography, Martin Luther University Halle-Wittenberg, Von-Seckendorff-Platz 4, 06120 Halle (Saale), Germany; mike.teucher@geo.uni-halle.de
[4] Department of Digital Geography, Institute of Geosciences and Geography, Martin Luther University Halle-Wittenberg, Von-Seckendorff-Platz 4, 06120 Halle (Saale), Germany; detlef.thuerkow@geo.uni-halle.de
* Correspondence: florian.thuerkow@hs-anhalt.de

Abstract

Stones in agricultural fields pose a recurring challenge, particularly due to their potential to damage agricultural machinery and disrupt field operations. As modern agriculture moves toward automation and precision farming, efficient stone detection has become a critical concern. This study explores the potential of thermal imaging as a non-invasive method for detecting stones under varying environmental conditions. A series of controlled laboratory experiments and field investigations confirmed the assumption that stones exhibit higher surface temperatures than the surrounding soil, especially when soil moisture is high and air temperatures are cooling rapidly. This temperature difference is attributed to the higher thermal inertia of stones, which allows them to absorb and retain heat longer than soil, as well as to the evaporative cooling from moist soil. These findings demonstrate the viability of thermal cameras as a tool for stone detection in precision farming. Incorporating this technology with GPS mapping enables the generation of accurate location data, facilitating targeted stone removal and reducing equipment damage. This approach aligns with the goals of sustainable agricultural engineering by supporting field automation, minimizing mechanical inefficiencies, and promoting data-driven decisions. Thermal imaging thereby contributes to the evolution of next-generation agricultural systems.

Keywords: stone detection; remote sensing; precision agriculture; thermal imaging; drone imagery; image processing; soil surface analysis; thermal inertia

Academic Editor: Lilong Chai

Received: 29 April 2025
Revised: 18 June 2025
Accepted: 23 June 2025
Published: 1 July 2025

Citation: Thürkow, F.; Teucher, M.; Thürkow, D.; Mohri, M. Stone Detection on Agricultural Land Using Thermal Imagery from Unmanned Aerial Systems. *AgriEngineering* **2025**, *7*, 203. https://doi.org/10.3390/agriengineering7070203

1. Introduction

Soil texture plays a crucial role in determining the quality and productivity of agricultural land [1,2]. A coarse texture with the high presence of stones can become problematic for both crop growth and the efficient operation of machinery [1,3–5]. In particular, large stones over 150 mm cause severe problems when present in more than 10% of the arable layer [1]. On the other hand, small stones can also cause substantial damage to machines [3,4]. Depending on their size and quantity, stones can reduce the effectiveness of agricultural machines by up to 50%, and even moderate amounts of cobbles or boulders can significantly hinder tillage operations [1].

Due to the continuous removal of stones from fields over recent decades, there are relatively few studies that have assessed the current extent of stone content in arable

soils [6]. Despite this, stony soils remain common in agricultural regions worldwide. In Western Europe, it is estimated that around 30% of cultivated land contains between 20 and 75% coarse fragments within the top 20 cm of soil [7,8]. In the Mediterranean basin over 60% of farmland is affected by high levels of stoniness [7,8]. Stoniness has also been reported to negatively impact the productivity of arable land in parts of the Middle East [9]. The issue is further emphasized by records documenting the collection of several tens of tons of stones per hectare from agricultural fields [10,11]. Additionally, modern stone-picking machines are designed to handle up to 50 tons of stones per hectare, underscoring the substantial amount of stony material that can be present in cultivated soils [12].

Various mechanical solutions have been developed to reduce the coarse fraction within the top layer of agricultural soils. These include machines that collect and remove stones from the field, on-site stone crushers, or systems that bury stones deeper within the soil profile [1,5]. These machines are highly specialized and, as a result, mostly are cost-inefficient [1,11,13]. Typically, expensive equipment is only accessible to large-scale farms or agricultural contractors, while for smaller farming operations, it is only profitable if fields are heavily affected by stoniness [1].

In contrast, on fields where stones occur only occasionally, investing in heavy-duty stone removal machines is rarely cost-efficient. In these cases, stones must often be removed manually. This involves workers systematically walking across fields to identify and remove larger stones—especially during off-season months—before they can damage seeding, tilling, or harvesting equipment [5,11]. However, manually screening large areas of farmland is both time-consuming and labor-intensive. For small-scale farmers, who often operate with tight profit margins, this approach can become economically unsustainable [14].

As digitalization continues to reshape agriculture, there is growing potential to integrate stone detection into precision farming practices. Modern agricultural machinery is already equipped with advanced sensors and systems capable of utilizing and visualizing digital geodata [15–17]. If obstacles such as stones can be detected before they interfere with agricultural machinery, the field work becomes significantly safer [18], while also minimizing equipment damage, reducing soil compaction, and lowering labor costs. This early intervention enhances overall efficiency and contributes to more sustainable farming practices. In this context, automated stone detection and mapping emerges as a promising advancement in the evolution of precision agriculture.

During the last two decades, the technological progress of Unmanned Aerial Systems (UAS) generally emerged [19] and thus also influenced the agricultural sector, especially in the continuously growing field of precision agriculture [20]. Based on well-documented reviews in the literature [21–26], the most common field applications of UAV in agriculture are crop health monitoring and disease detection, growth monitoring and yield estimation, irrigation management, assessments of soil properties and weed management. While there exists a plethora of scientific research on yield and biomass monitoring, as well as diseases detection, the minority of research is published on the potential of thermal sensors [27,28] with recently an increasing number focusing on object detection [29,30]. One study utilized thermal imaging to investigate plant stress [31]. Additionally, another study investigated the potential of UAS-thermal imaging for crop abiotic stress monitoring [32]. In terms of boosting UAS-thermal imaging techniques in precision agriculture, both studies concluded that data-intensive procedures, experts and skilled personnel, as well as robust tools are required to increase the adoption of thermal imaging [31,32].

The objective of this study is to assess the general applicability of Unmanned Aerial System-carried (UAS-based) thermal sensors for stone detection in agricultural fields. The goal is to reliably identify stones not only on flat surfaces, but also in more complex microterrain—such as potato, peanut or asparagus ridges—and in areas where stones are partially

buried. In such conditions, LiDAR systems may fail to capture stones due to limited surface elevation contrast. Similarly, conventional RGB imagery can lack sufficient visual contrast, as dust-covered stones often blend with the surrounding soil. In addition, soil clods can closely resemble stones in both shape and appearance, which increases the likelihood of false detections. Thermal cameras, on the other hand, are increasingly integrated into agricultural machinery for applications such as yield estimation or the detection of plant diseases [33], and they represent a more accessible and practical solution than the costlier and less widespread LiDAR systems. By leveraging temperature differences between materials, thermal imaging offers a promising alternative for a more accurate stone detection method.

This study aims to identify the optimal conditions for reliably distinguishing between soil and stone surfaces using thermal imaging, both in controlled laboratory settings and under field conditions. Specifically, rocks generally have a higher volumetric heat capacity than soil, leading to slower heating and cooling cycles [34–36]. This difference in thermal behavior should lead to a significant contrast in surface temperatures, with stones showing more stable temperatures over time and surrounding soil responding more rapidly to environmental changes. Due to variable management practices on the field, the soil texture and surface is often very heterogeneous, including soil clods on fields. Additionally, soil moisture content influences soil temperature, soil reflectance and soil heat storage capacity, with higher soil moisture content mitigating soil temperature differences between day-time and night-time and higher heat storage capacity [37–39]. Thus, the following hypotheses will be investigated:

(1) Thermal inertia effects lead to significantly higher surface temperatures for stone objects than surrounding soil;
(2) Clods indicate no significant temperature difference compared to the surrounding soil due to the same parent material and thus comparable thermal behavior;
(3) Higher soil moisture contents will significantly increase the magnitude of the temperature difference between stones and soil;
(4) Thermal inertia effects lead to the better detectability of stones on agricultural fields during daily phases of rapid changes in ambient air temperature, e.g., sunrise and sunset, compared to midday. Specifically, the most significant disparities occur during the sunset phase.

2. Materials and Methods

To explore the applicability of UAV-based thermal imaging for detecting stones, a field trial was conducted prior to a series of controlled laboratory experiments. Later ones were conducted to investigate the suitability of stone detection under easily controllable varying environmental conditions. Laboratory experiments and field trials were conducted from March to June 2021 within the context of the project AgriSens DEMMIN 4.0.

2.1. Field Experiment

The field experiment aimed to generally evaluate the potential of thermal imagery for stone detection on agricultural fields, and was conducted on 30 March 2021 on a field near the village Bentzin in Mecklenburg-Vorpommern (Germany). The trial encompassed data collection during the morning, around midday and in the evening (see Table 1). The data collection was conducted using a DJI M300 RTK drone equipped with a DJI Zenmuse H20T radiometric thermal imaging camera (SZ DJI Technology Co. Ltd., Shenzhen, China). The spectral range of the camera is 8–14 µm, the focal length 13.5 mm, and the sensor resolution 640 × 512 pixels. The drone maintained a stable flight at an altitude of approximately 50 m, with an average flight speed of around 1 m/s. In terms of cultivation, the field was prepared

for potato cultivation, so the soil surface showed typical mounding structures. The field was prepared for potato harvesting, featuring a hill structure characteristic of potato cultivation. The surface was free of vegetation, allowing rocks to be visually distinguishable from the soil. On all three days prior to the field experiment, rain was recorded by the two nearest weather stations within the German meteorological network (Anklam and Greifswald [40]). The temperature and relative humidity during the flights were determined by averaging the data from the two weather stations.

Table 1. Details on the conditions during the field experiment.

Date (Time)	Time of the Day	Air Temperature [°C]	Relative Humidity [%]	Soil Moisture [%]
30 March 2021 (06:30–07:00)	Morning	10.7	83.0	~20
30 March 2021 (10:45–11:30)	Midday	17.8	63.6	~20
30 March 2021 (20:30–21:00)	Evening	13.4	76.8	~20

From each flight, 15 images were selected and one individual stone was evaluated per image. Temperature data were extracted using the DJI Thermal Analysis Tool 3 (Windows version 3.4.0, DJI, Shenzhen, China) software. The distance to the object was set to the maximum allowable limit of 25 m. The emissivity was set to an average value between moist and dry soil, as indicated in the emissivity table from ThermoWorks [41].

Within the software, a circular selection tool was used to define the stone, and the mean temperature of all pixels within the circle was recorded. To compare this with the surrounding soil, a square selection was placed over the adjacent soil area that exhibited the highest temperature, ensuring that the warmest portion of the soil was used for comparison with the stone.

2.2. Experimental Setup

Based on the preliminary experiences and findings of the field trial, a series of laboratory experiments took place from 4 to 10 June 2021 in a temperature-controlled climate chamber at the geoecological laboratory of the Institute of Geosciences and Geography at Martin Luther University. The setup consisted of two plastic containers, each approximately 55 × 35 × 35 cm in size, filled with around 50 L of soil (see Figure 1). The soil exhibited a high proportion of gravel and sand in the particle size fraction > 0.063 mm, and a low content of fine particles (silt and clay) in the fraction < 0.063 mm. In each container, two large stones collected from an agricultural field were placed, along with a soil clod, which is a compact, naturally formed or manually shaped lump of soil that resembles a stone in appearance but consists entirely of compressed soil particles.

A calibration plate made of aluminum was centrally positioned between the two containers. This plate quickly aligns with the ambient air temperature and serves as a reference to verify the temperature readings of the thermal camera. Additionally, temperature sensors (RS PRO Type T, Radionics Ltd., Dublin, Ireland) were installed to monitor the ambient air temperature and surface temperature of the calibration plate in the range from 40 to +125 with precision of ±0.5 °C and from +125 to +350 within the tolerance of ±0.4%. Sensor data were recorded using a PerfectPrime TC0520 thermal logger (PerfectPrime, New York, NY, USA). Artificial lighting was provided by a Double Halogen daylight lamp with a luminous flux of 8800 lumen, mounted at a height of 2 m

with a beam angle of 30°, which revealed an illuminance area of 0.9 m^2 with 9754 lux. To minimize external temperature influences and simulate natural soil conditions as accurately as possible, the containers were fully insulated with Styrofoam on the sides and bottom. Soil moisture monitoring was carried out using the ML3 ThetaProbe soil moisture sensor (Delta-T Devices Ltd., Cambridge, UK). The ML3 ThetaProbe measured the volumetric water content and soil temperature in the range of 0 to 0.5 m^3 m^{-3} and to an accuracy of 1%. Approximately 1.5 m above the experimental setup, a drone-mounted imaging system was installed to capture images from a top-down perspective. The drone (DJI M300 RTK) was the same as that used during the field experiment.

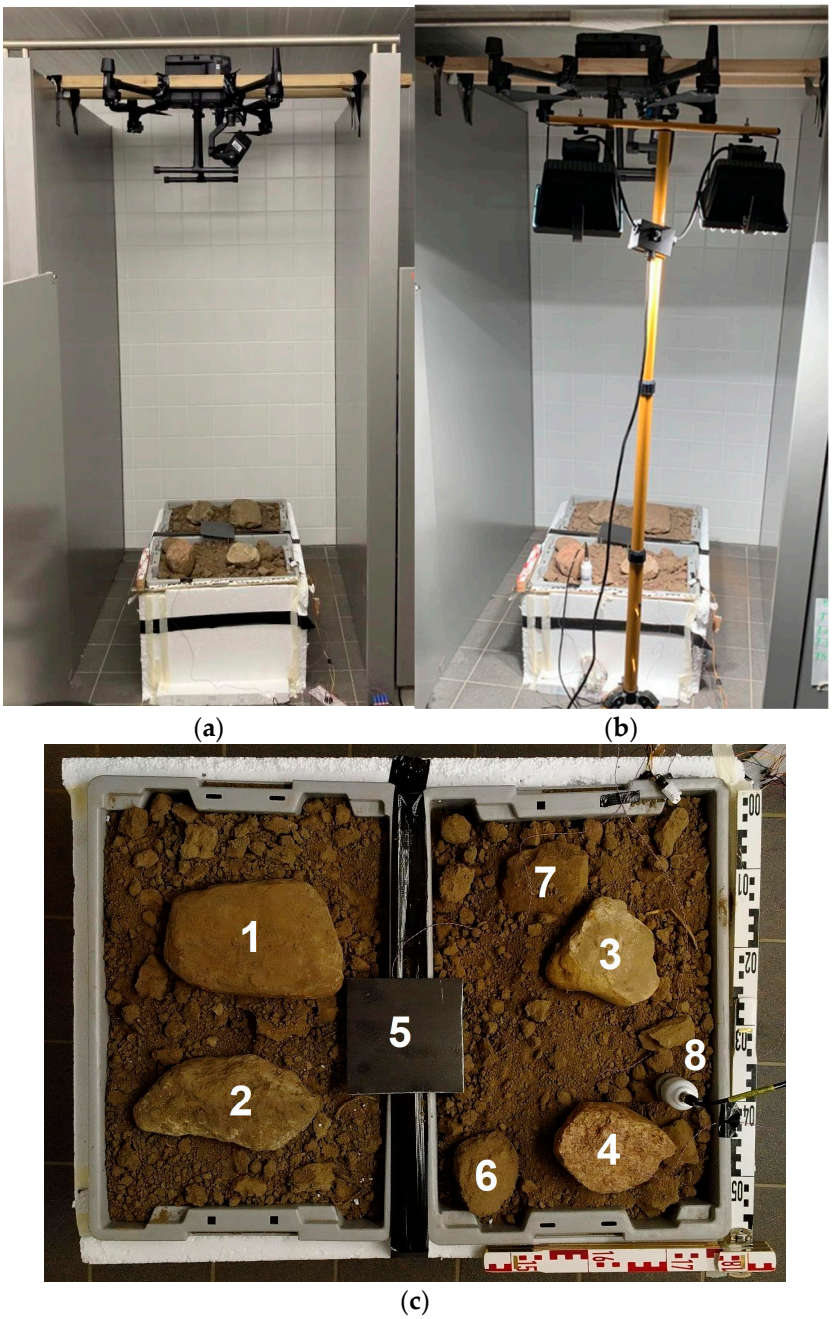

Figure 1. Experimental setup in the climate chamber under controlled conditions. (**a**) Setup without artificial light; (**b**) setup with artificial light; (**c**) the soil containers with numbers 1 to 4 indicating stones, number 5 referring to the calibration plate, numbers 6 to 7 pointing at soil clods, and number 8 marking the soil moisture sensor.

Thermal images were recorded at one-minute intervals to monitor temperature variations over time. However, only every fifth image was included in the analysis, as changes between consecutive images were minimal. This approach reduced the amount of data to be analyzed and allowed for the selection of a greater number of sample pixels.

2.3. Experimental Conditions

The experimental conditions were designed to replicate realistic temperature dynamics occurring during usual stone collection periods (October–March) in agriculture, focusing on the effects of radiative heating (sunlight) and soil moisture. This management period during an agricultural management year offers no to low plant coverage and thus is most suitable for UAV-based stone detection. By varying moisture levels, temperature trends (cooling, warming, stable), and exposure to radiation, the experiments aimed to capture key thermal processes relevant to soil and stone surfaces. The inclusion of both dry and moist conditions allowed for the assessment of moisture's role in heat retention and dissipation. Additionally, gradual cooling and warming phases simulated the natural temperature fluctuations that occur under field conditions. A stable temperature scenario with radiative input was also tested to analyze heat absorption under constant conditions. The specific temperature changes and durations for each experimental condition are summarized in Table 2.

Table 2. Overview of the experimental conditions. Temperature changes were monitored linearly by the control unit of the climate chamber.

Experimental Condition	Date and Duration [h]	Initial Air Temperature [°C]	Final Air Temperature [°C]	Soil Moisture [%]
Dry + Cooling (D + C)	4 June 2021, 7 h	16.9	10.6	<10
Dry + Stable + Light (D + S + L)	7 June 2021, 4 h	17.3	17.6	<10
Moist + Stable + Light (M + S + L)	8 June 2021, 4 h	17.6	17.5	~20
Moist + Cooling (M + C)	9 June 2021, 7 h	17.1	11.0	~20
Moist + Warming (M + W)	10 June 2021, 7 h	10.6	16.8	~20

2.4. Image Quality Control

Images were inspected for disruptions caused by sensor placement. Affected images were replaced with the immediately preceding or succeeding image (±1 min) to maintain consistency. Further, the image sequences were examined for major perspective shifts caused by battery replacements and sensor placement. This was done by visually comparing the first and last images of each photo series, which spanned between 4 and 7 h. Since no significant deviations were identified, the sample point coordinates were defined once for the entire series of experiments.

2.5. Determination of Sample Pixels

For the image analysis, sample points were selected using a semi-randomized approach to ensure a balanced distribution across the image. In each image half corresponding to the left and right container, a mask was created to distinguish soil from stones. Within

these masked regions, 20 random sample points were selected per category, resulting in an initial total of 40 sample points for soil and 40 for stones per image.

To maintain consistency across the image series, sample point positions were visually inspected in the first and last images of each series. Points too close to category boundaries, where minor shifts in the image's field of view could lead to misclassification, were excluded. After balancing the sample points across both halves, 26 sample points remained for soil and 26 for stones (13 in each half per category).

Additionally, five manually placed sample points were added in the central area of the calibration plate and another five in the area of the soil clod. In total, 36 sample points were defined. To reduce the influence of localized extremes, each sample point was expanded into a 5 × 5 pixel square, with the originally selected pixel as the center. This resulted in 650 pixels for soil, 650 pixels for stone, 125 pixels for the calibration plate, and 125 pixels for the soil clod. The final sample point positions can be seen in Figure 2.

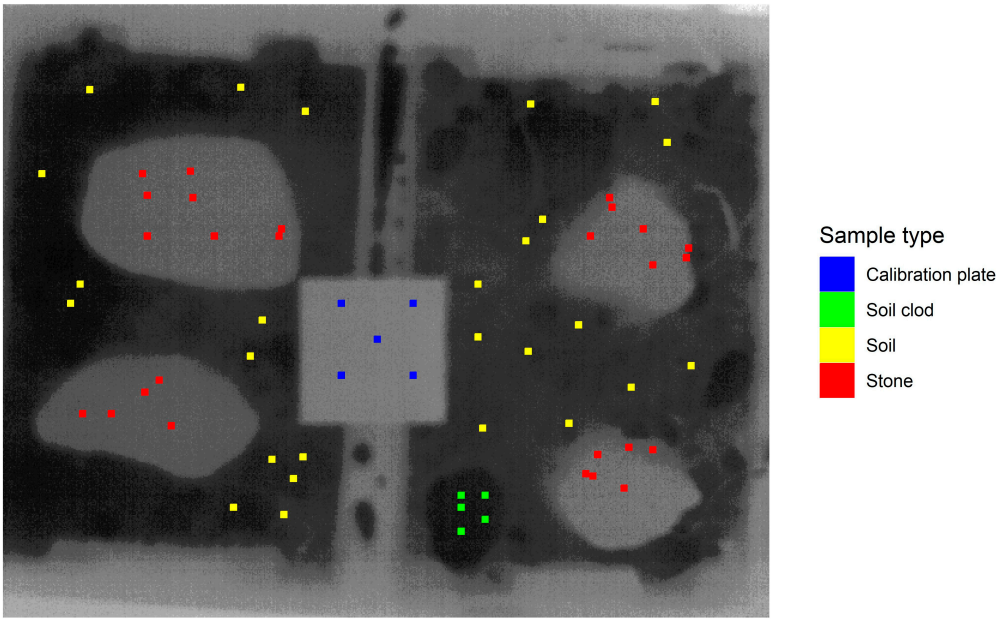

Figure 2. Distribution of sample points plotted on an exemplary thermal image displayed in grey scale.

2.6. Data Analysis and Statistical Testing

Temperature data from each pixel were extracted using the software DJI Thermal SDK v1.6 20240926 [42], which produced.raw files. These raw thermal data files were then converted into text format with corresponding spatial coordinates. This conversion as well as the statistical analysis was performed in R Studio Version 2025.05.1+513 [43–50]. To assess statistically significant differences, the data were first tested for normality. Depending on the outcome, either parametric or non-parametric statistical tests were applied. In addition, general linear models were used to assess the effects of temperature changes on the difference between stone and soil temperatures. Results with a p-value < 0.05 were considered statistically significant.

3. Results

3.1. Field Experiment

In the field experiment, no statistically significant temperature differences between the stones and the surrounding soil were observed during the morning and midday periods (see Table 3). In contrast, the evening measurements showed a clear and statistically significant temperature elevation in the stones compared to the soil.

Table 3. Temperature differences between stones and field soil during different times of the day.

Time of the Day	Statistical Test	Mean (Mn) or Median (Md) Difference Stones and Soil [K]	Standard Deviation (SD) or Interquartile Range Q1–Q3 (IQR)	Test Statistic (Degrees of Freedom)	*p*-Value *
Morning	*t*-test	0.08 (Mn)	0.48 (SD)	0.65 (14)	0.529
Midday	*t*-test	0.17 (Mn)	2.17 (SD)	0.31 (14)	0.762
Evening	Wilcoxon	2.2 (Md)	1.55–2.55 (IQR)	120 (na)	<0.001

* Testing whether the mean or median difference is significantly different from 0. na = not applicable.

Examining the thermal images of a representative field section containing a large stone, distinct patterns throughout the day become visible (see Figure 3). In the morning, the thermal image showed minimal contrast, indicating that both the stone and the surrounding soil had similar temperatures following the cool night. Around midday, temperature differences became more apparent, though not specifically between the stone and the soil. Instead, variations were visible across the terrain; sloped areas at the potato ridges facing the sun exhibited higher temperatures due to solar exposure, while the stone cast a visible shadow, appearing as a colder region. In the evening, the stone distinctly stood out as a warmer object.

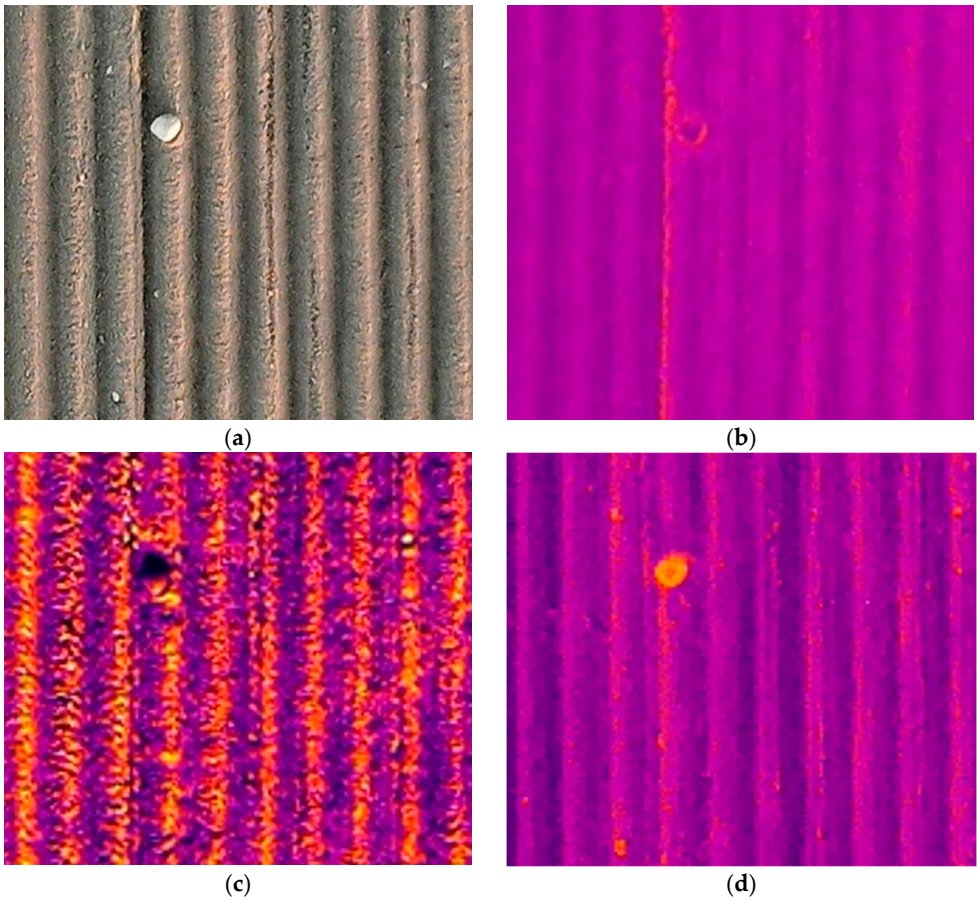

Figure 3. (**a**) RGB image, (**b**) thermal image in the morning at 7:06 a.m., (**c**) thermal image around midday at 11:12 a.m. and (**d**) thermal image in the evening at 20:28 p.m. of a stone in the field. Temperature scales are not displayed, as the thermal range varies between images and the focus lies on the relative differences between the stone and the surrounding soil.

3.2. Comparison of Thermal Camera and Surface Temperature Measurements

Comparing temperature measurements on the calibration plate, recorded by both the surface temperature sensor and the thermal camera, revealed a gradually increasing discrepancy over time (see Figure 4). While the surface sensor readings closely matched the set temperature of the climate chamber, the thermal camera showed increasing deviations. During periods of decreasing ambient temperature, the camera underestimated surface temperature, and during rising temperatures, it overestimated. Based on these observations, further analyses are based on temperature differences rather than absolute values.

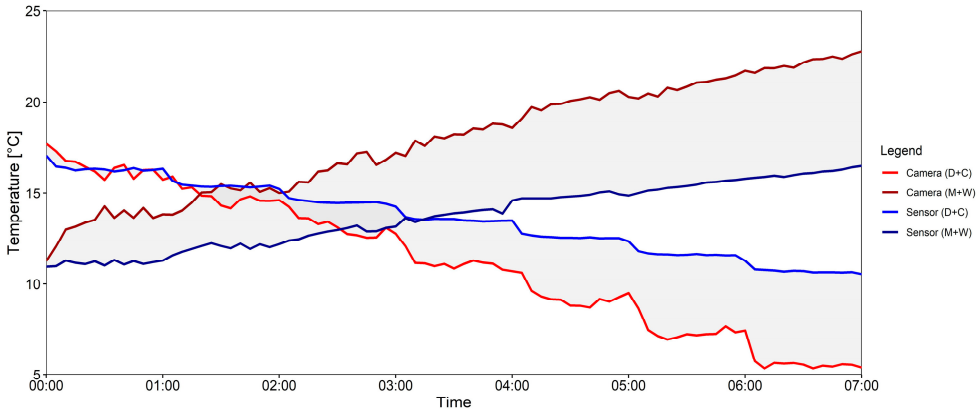

Figure 4. Temperature measurements on the calibration plate taken by the thermal camera (red) and the surface temperature sensors (blue) for two of the five experimental conditions (Dry + Cooling and Moist + Warming).

3.3. Temperature Differences Between Stones and Soil

In the experiment with cooling ambient air temperature and moist soil, the stones remained consistently warmer than the surrounding soil (see Figure 5). The temperature difference between the two surfaces gradually increased over time as the ambient temperature decreased. When soil moisture was low, stones remained warmer than the soil for most of the experiment; however, the temperature difference was comparatively small. Under both = moist and dry soil conditions, rather than following a linear trend, the differences fluctuated around 0.5 K, with periods of steeper increases followed by more gradual cooling phases. Notably, the rapid rise in fluctuations aligned precisely with a sharp drop in ambient air temperature, which occured periodically, decreasing by approximately 1 K every hour.

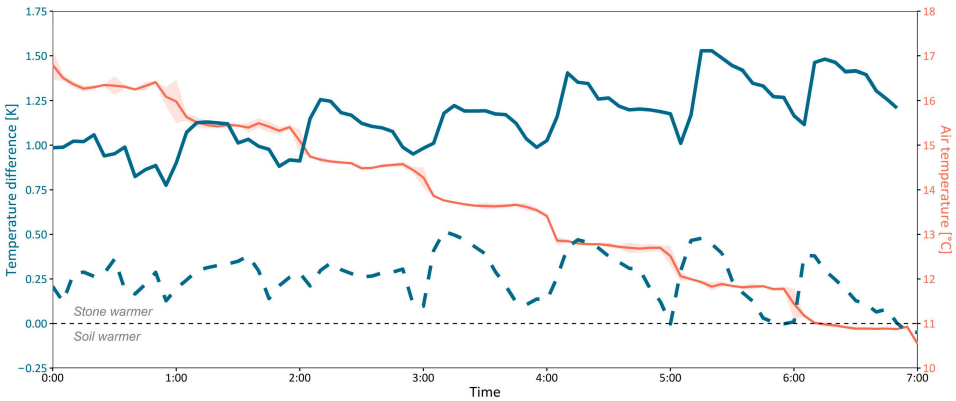

Figure 5. Temperature difference between the stones and the soil for moist soil conditions (blue solid) and dry soil conditions (blue dashed) measured by the thermal camera and mean surrounding air temperature (red) under the M + C and D + C experimental conditions.

In the experiment with gradual ambient warming and moist soil, the stones generally exhibited higher temperatures than the surrounding soil (see Figure 6). Only during the initial half hour was the soil slightly warmer. The overall temperature difference was less pronounced than in the cooling scenario. Nevertheless, even under warming conditions, the difference between stone and soil temperatures increased steadily, though with smaller fluctuations than those observed during cooling.

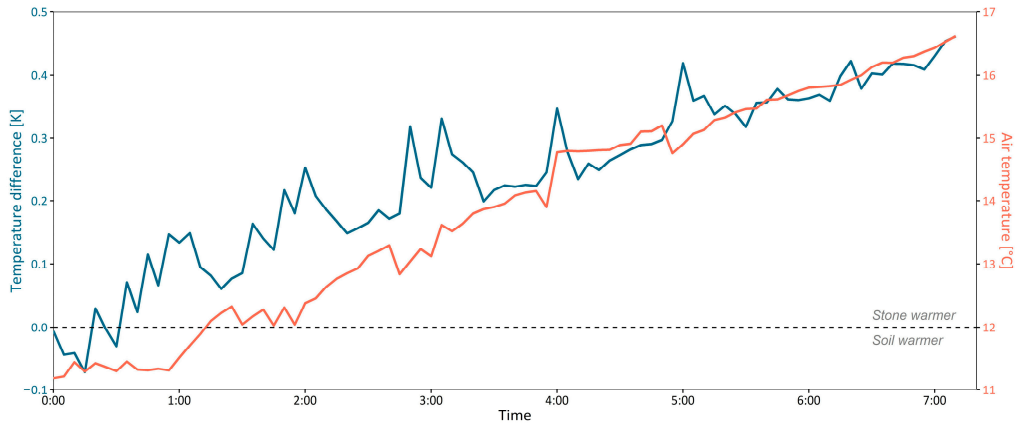

Figure 6. Temperature difference between the stones and the soil for moist soil conditions (blue solid) measured by the thermal camera and surrounding air temperature (red) during the moist and warming (M + W) experimental conditions.

The experiments using a light source during the first two hours showed an initial warmer ambient temperature of around 19.5 °C. Once the light was switched off, the temperature quickly stabilized at around 17.5 °C (see Figure 7). In the experiment with moist soil, the stone surface remained consistently warmer throughout the entire experiment. The temperature difference was most pronounced shortly after the lights were turned off, as the ambient air cooled. In contrast, under dry soil conditions, the soil was initially warmer than the stone surface. However, as the ambient air temperature dropped, this trend reversed, with the stones becoming warmer than the soil. Despite this shift, the temperature difference during the dry soil conditions remained smaller than under moist soil conditions.

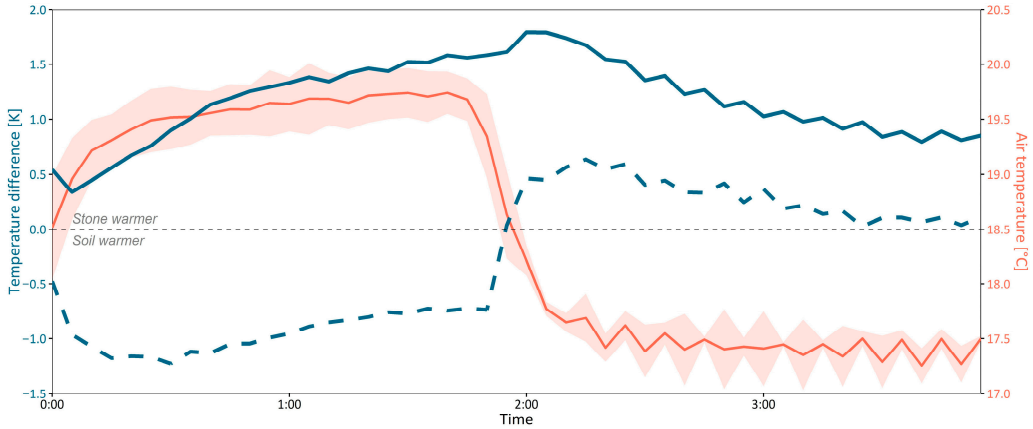

Figure 7. Temperature difference between the stones and the soil for moist soil conditions (blue solid) and dry soil conditions (blue dashed) measured by the thermal camera and mean surrounding air temperature (red) during the M + S+L and D + S+L experimental conditions.

Under all five experimental conditions, the stones exhibited higher median temperatures than the soil (see Table 4). The largest temperature difference was observed under

moist soil conditions with stable temperature and light exposure (M + S + L), where stones were significantly warmer than soil (M + C), with a median difference of 1.21 K. Under moist conditions with ambient cooling, the stones showed a similarly high median temperature difference of 1.17 K. Under dry soil conditions, the temperature difference between soil and stones was still positive, though much smaller, with a median of 0.28 K for cooling ambient temperature (D + C) and 0.03 K under the stable temperature regime (D + S + L). In the latter case, the interquartile range was highly variable, and also included instances in which the soil was warmer than the stones. The experiment with warming temperature also had a relatively small median difference of 0.25 K (M + W). Overall, the median temperature differences between stones and soil were significantly greater than zero in all experiments. However, the interquartile ranges showed considerable variability, indicating different magnitudes of temperature differences across experiments.

Table 4. Temperature differences between stones and soil under various experimental conditions.

Experimental Conditions	Median Difference Stones and Soil [K]	Interquartile Range (Q1–Q3)	Wilcoxon W-Statistic	*p*-Value (Wilcoxon Signed-Rank Test) *
Dry + Stable + Light	0.03	−0.91–0.27	329	<0.01
Moist + Warming	0.25	0.15–0.36	3796	<0.001
Dry + Cooling	0.28	0.14–0.34	3637	<0.001
Moist + Cooling	1.17	1.01–1.26	3486	<0.001
Moist + Stable + Light	1.21	0.90–1.48	1176	<0.001

* Testing whether the median difference is significantly different from 0.

3.4. Temperature Differences Between Soil Clods and Stones

The differences between stones and the soil clod were generally similar to the differences between stones and soil. The Wilcoxon signed-rank test confirmed that temperature differences between stones and soil clods were all statistically significant (see Table 5). However, the directions of the effects differed across the experimental conditions. While under the Dry + Stable + Light condition, stones were slightly cooler than soil clods, stones were warmer under all other experimental conditions. The greatest temperature difference was observed under Moist + Cooling conditions, where stones were notably warmer than soil clods. Similarly, the Moist + Stable + Light also showed the considerable warming of stones compared to soil clods.

Table 5. Temperature differences between stones and soil clods under various experimental conditions.

Experimental Conditions	Median Difference Stones and Soil Clods [K]	Interquartile Range Q1–Q3 [°C]	Wilcoxon W-Statistic	*p*-Value (Wilcoxon Signed-Rank Test) *
Dry + Stable + Light	−0.14	−0.91–0.22	311	<0.01
Moist + Warming	0.30	0.27–0.38	3828	<0.001
Dry + Cooling	0.49	0.40–0.68	3655	<0.001
Moist + Cooling	1.63	1.42–1.90	3486	<0.001
Moist + Stable + Light	1.13	0.92–1.33	1176	<0.001

* Testing whether the median difference is significantly different from 0.

3.5. Effect of Soil Moisture on the Temperature Differences Between Stones and Soil

Experiments with higher soil moisture produced larger differences between stone and soil surfaces (see Figure 8). For cooling ambient conditions, the Welch Two Sample *t*-test revealed that the temperature difference under moist conditions was significantly greater than that under dry conditions (t(154.34) = −37.0, *p*-value < 0.001, 95% confidence interval −0.95 to −0.86 K). Under dry conditions, stones were on average only 0.25 K warmer than the surrounding soil, whereas under moist conditions, the temperature difference amounted to 1.16 K (see Figure 8a).

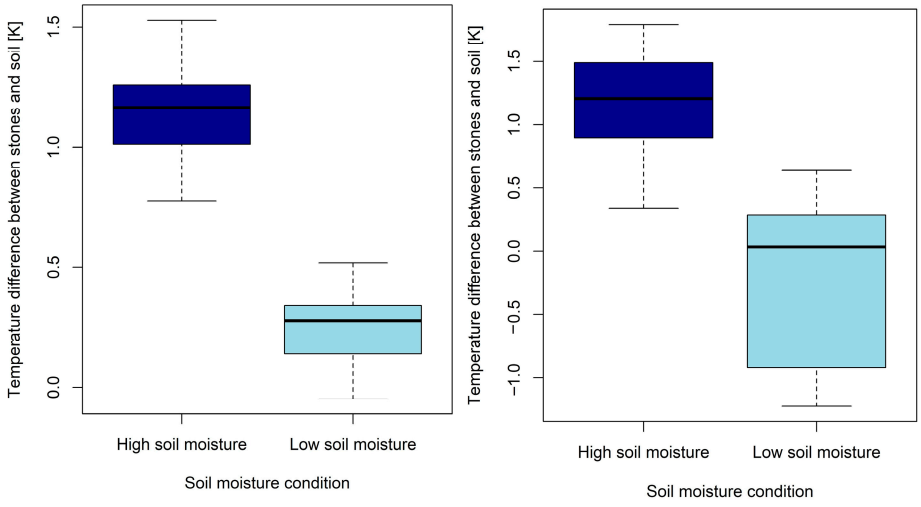

(**a**) (**b**)

Figure 8. Boxplots comparing temperature differences for (**a**) cooling ambient air temperature conditions and (**b**) stable air temperature conditions with initial lighting. Boxes show the interquartile range, with the median as a horizontal line. The dashed whiskers extend to the most extreme values with 1.5 times the interquartile range from the quartiles.

Under stable temperature conditions with initial lighting, the Wilcoxon rank-sum test produced similar results to the Welch *t*-test. The temperature difference between soil and stones was significantly larger under moist soil conditions (W = 23, *p*-value < 0.001). The median temperature differences were −0.30 K for the low soil moisture and 1.18 K for the high soil moisture conditions (see Figure 8b).

3.6. Effect of Rapid Temperature Change on the Difference Between Stone and Soil Temperature

The relationship between the lagged absolute ambient temperature change rate and the temperature difference between stones and soil was not consistent across all experimental conditions (see Figure 9).

Two experimental conditions (Dry + Cooling and Dry + Stable + Light) featured a significant positive effect of ambient temperature change rate on the temperature difference between stones and soil. Under the Dry + Cooling condition, the predictor had a significant effect (β = 0.39, SE = 0.10, t(80) = 3.81, $p < 0.01$), explaining 15.35% of the variance (R^2 = 0.15). Under the Dry + Stable + Light condition, the effect was even stronger (β = 1.65, SE = 0.55, t(42) = 3.01, $p < 0.01$), with the model accounting for 17.69% of the variance (R^2 = 0.18). Both general linear models were statistically significant.

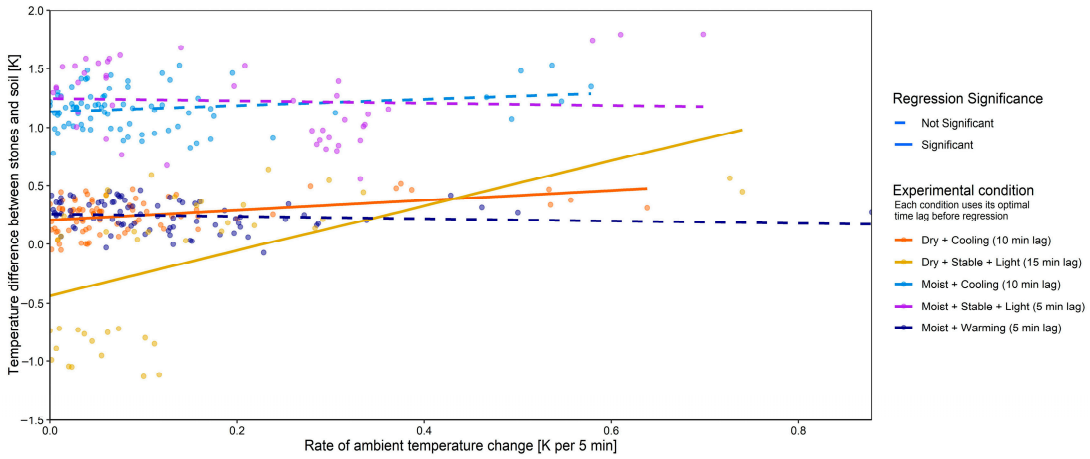

Figure 9. Relationship between the absolute rate of ambient temperature change and the temperature difference between stones and soil across five experimental conditions. Each condition was analyzed using the time lag that produced the most pronounced effect in the regression, as specified in the legend. Solid lines represent statistically significant regressions ($p < 0.05$), while dashed lines indicate non-significant relationships.

In contrast, for the experiments with moist soil, the ambient air temperature change rate had no significant effect on the temperature difference between stones and soil. The Moist + Cooling model showed no significant relationship ($\beta = 0.26$, SE = 0.15, $t(78) = 1.73$, $p = 0.09$) and explained only 3.71% of the variance ($R^2 = 0.04$). Similarly, under the Moist + Stable + Light condition, the effect was non-significant ($\beta = -0.26$, SE = 0.29, $t(44) = -0.90$, $p = 0.37$), with the model explaining just 1.81% of the variance ($R^2 = 0.02$). Lastly, the Moist + Warming condition also produced no significant effect ($\beta = -0.08$, SE = 0.11, $t(83) = -0.75$, $p = 0.46$), and the model accounted for less than 1% of the variance ($R^2 = 0.01$).

Overall, significant positive effects of temperature change rate on the temperature difference between stones and soil were observed only under dry conditions (D + C and D + S + L), whereas moist conditions (M + C, M + W, and M + S + L) showed no meaningful relationship.

4. Discussion

4.1. Temperature Differences Between Stones and Soil

When aiming to distinguish individual objects from their backgrounds using thermal imaging, strong temperature contrasts within the image are beneficial. The greater the differences in thermal conductivity and heat capacity between materials, the more distinct the resulting thermal contrast becomes. Together with the material's density, these two properties define the thermal inertia [51]. While nonporous rocks typically have a specific heat capacity around 900 J kg^{-1} K^{-1} [52], the water present in moist soil has a much higher heat capacity of over 4000 J kg^{-1} K^{-1}, while air has one of only about 1000 J kg^{-1} K^{-1}. Additionally, the organic content of soil can increase its heat capacity [53]. Therefore, moist soil should retain more heat than dry soil or rock. However, when considering volumetric heat capacity—which accounts for the material's density—rocks emerge as superior [34]. Their higher density allows them to store more thermal energy per unit volume, making them slower to cool and more effective at retaining warmth compared to either dry or moist soil. Furthermore, stones have a higher thermal conductivity than soil, enabling them to absorb and distribute heat more efficiently [54]. In contrast, soil has a lower thermal conductivity due to its higher air content and lower density, making it less effective in heat transfer [35,54].

In the first half of the experiment with additional lighting, the dry soil initially exhibited higher surface temperatures than the stones. This changed once the light source was turned off and the ambient air temperature dropped by a few degrees—at which point the stones retained more heat. This behavior reflects the dry soil's lower thermal inertia, allowing it to respond quickly to temperature changes, while the stones, with their greater heat storage capacity, accumulated thermal energy more gradually and released it more slowly. This is inline with the results revealed by satellite-based thermal inertia mapping, e.g., for soils moisture [39,55,56] and geology [57]. Similarly, in the initial phase of the Moist + Warming experiment, moist soil showed slightly higher temperatures than the stones. This may be attributed to the soil's lower thermal conductivity, which limits heat transfer into deeper layers, resulting in a faster rise in surface temperature. In contrast, the stone likely conducted heat away from its surface into its interior. However, as the experiment progressed, the stone surface became warmer than the moist soil, likely due to evaporative cooling effects at the soil surface, which reduced its temperature despite ongoing warming. A similar effect was observed in the experiment with moist soil under stable ambient conditions and initial lighting, where stones maintained higher surface temperatures. This was likely due to evaporative cooling reducing the soil's surface temperature relative to the more thermally stable stones. Under cooling conditions, both with dry and moist soil, the stone surfaces consistently remained warmer than the surrounding soil. This is consistent with their higher thermal inertia, allowing them to release stored heat more gradually than the soil. In general, the results show that stone surfaces were significantly warmer than the surrounding soil, especially under moist soil conditions.

In field conditions, stones were significantly warmer than the surrounding soil only in the evening as ambient temperatures dropped. This confirms that they retain and accumulate heat throughout the day, resulting in a more pronounced temperature contrast in the evening. However, in the morning, stones were not consistently colder than the soil, likely due to the continuous evaporation from the moist soil and the fact that stones absorbed a substantial amount of heat over the preceding days, which they retained.

In summary, while the difference in thermal inertia between soil and stone explains why stones remain warmer during periods of decreasing ambient temperature, evaporative cooling also plays a significant role under warming conditions. Therefore, the first hypothesis can only be partially confirmed—specifically for moist soil under cooling conditions. Under other ambient scenarios, the temperature differences appear more complex and are likely influenced by evaporative effects.

The second hypothesis, predicting similar thermal behavior between soil and soil clods, is generally supported by the results. Although under one experimental condition the median temperature of the clods was slightly higher than that of the stones—despite stones being warmer than the surrounding soil—the overall difference was minimal. As seen in the graphical data (Appendix A Figures A1–A5), the temperature trends of soil and clods closely align, indicating that their thermal behaviors remained largely comparable.

Differences in thermal inertia between stones and soil are also used in other applications, such as in archeology. In particular, ancient building structures, such as houses or roads, can be detected using infrared imagery [34,58]. In the case of subsurface architecture, structures like walls or foundations, which retain heat differently than the surrounding soil, can be identified through thermal imagery [34]. These thermal contrasts arise because the buried structures, with their distinct material properties, exhibit a slower or different rate of cooling compared to the surrounding soil, making them visible in the thermal image, even if they are not visible on the surface [34].

Overall, the results from both the experiments and the field study—as well as observations from practical applications—indicate that the ability of stones to retain heat longer

can be effectively captured using thermal imaging, particularly under conditions of high soil moisture and decreasing ambient air temperature.

4.2. Effect of Soil Moisture

The experiments in this study reveal that, under both warming and cooling ambient conditions, the temperature contrast between stones and soil was largest when soil moisture was high. This can be attributed to the fact that the stones were generally warmer than the soil, and that the evaporative cooling additionally cooled the moist soil [59]. As water evaporates from moist soil, energy is required to drive the phase transition from liquid to vapor [60]. This energy—the latent heat of vaporization—is extracted from the surrounding environment [60]. As a result, less energy is available to be released as sensible heat, leading to a net cooling of the soil surface [60]. This process explains why the observed temperature difference between stones and moist soil can be larger than between stones and dry soil.

The link between soil surface temperature and soil moisture has already been noted in earlier studies [37,38]. A simple laboratory experiment using an infrared camera to monitor the surface temperature of different soil types at different initial moisture contents clearly demonstrated that also after 7 days, soils with a high initial moisture content of around 40% were approximately 10 °C cooler than soils with a lower initial moisture content of about 12% [39]. The significance of this relationship is further emphasized by numerous remote sensing approaches at medium and large scales that utilize surface temperature as a key indicator of soil moisture [57,59,61–65]. In particular, the capacity of soil moisture to amplify surface temperature variability has found practical application, notably in archeological research [34,58]. In this context, the detection of ancient stone infrastructure has proven more effective under relatively moist soil conditions. The authors observed distinct thermal contrasts between buried stone features and the surrounding soil, suggesting that moisture-driven differences—potentially influenced by subsurface structures—enhance their visibility through thermal imaging techniques [58]. Correspondingly, another study found that under prolonged arid conditions, when no precipitation has occurred since the previous spring, soil and stone surfaces exhibit nearly identical thermal properties. In such a case, thermal surveys—even when conducted at night—yield minimal archeological visibility due to the lack of differential heat retention [34]. The authors therefore concluded that the soil moisture is a highly important factor in aerial thermography, but also noted that successful detection requires buried structures of sufficient sizes or extents, as smaller features such as individual fieldstones may remain thermally indistinct [34].

The results of the present study are consistent with both theoretical expectations and empirical evidence from laboratory as well as field research across disciplines. They highlight that soil moisture plays a significant role in thermal imaging. Therefore, the third hypothesis—that soil moisture amplifies the thermal contrast between stones and the surrounding soil—can be confirmed.

4.3. Effect of Rapid Temperature Changes

The theory of thermal inertia suggests that different materials heat and cool at varying rates, which supports the expectation of greater temperature differences between stones and soil during periods of rapid ambient air temperature fluctuations [51]. However, the results indicate that this behavior is more complex and highly dependent on environmental conditions. A possible explanation is that under moist soil conditions, the absolute thermal contrast between stones and soil was generally higher, which diminished the relative influence of short-term ambient air temperature fluctuations. In contrast, when the soil was dry, overall temperature differences were smaller, making the setup more responsive to rapid changes in air temperature. This interpretation aligns with a conceptual and

numerical climate model, which shows that in moist environments, surface temperature dynamics are predominantly governed by latent heat fluxes [66]. As a result, the role of thermal inertia becomes negligible [66].

Also in the archeological context, the most effective moment for thermographic imaging with drones turned out to be directly after sunset, when surface temperature contrasts were strongest [34,58]. Besides this, the fact that same study found that a sharp sequence of heating and cooling proved more relevant than the absolute range of diurnal temperature variation.

Overall, the findings suggest that the rate of temperature change plays a more critical role in environments where temperature contrasts between stones and soil are smaller. Thus, the fourth hypothesis can be considered partially confirmed.

4.4. Opportunities and Limitations of the Study

Although the findings provide valuable insights, several limitations must be considered when interpreting the results. Absolute temperature values could not be used, as during the experiments under controlled conditions, the heat emitted by the drone itself may have affected the thermal measurements, potentially introducing bias. Additionally, the temperature extraction tool used for analyzing field data did not allow for setting the actual drone flight height of 50 m, as the software had a maximum limit of 25 m. This discrepancy may have affected temperature readings and their accuracy. Further, the field trial was conducted on a potato field with an uneven surface, where hilly structures created slopes that were more exposed to sunlight due to their angle. This uneven exposure may have influenced temperature distributions across the field. Future studies should incorporate mitigation strategies to reduce inaccuracies. These measures include, among others, (1) keeping a minimum distance between the drone and target surface to reduce heat interference, (2) using calibration targets in the scene for temperature correction as also suggested in [27], and (3) terrain mapping to adjust for elevation effects.

Also, stones located beneath the soil surface were not considered in the analysis, which could have influenced the overall understanding of temperature differences between stones and soil. However, as shown by previous studies [34], rocky areas—even if buried by a layer of soil—can be detected. The ability to identify larger rocks even if only a part is visible on the surface is highly important in the agricultural context, as large boulders can strongly damage machinery [3,4,67]. During preliminary tests, UAS-based ground penetrating radar (GPR) was tested once, with unsatisfying success, due to complex constraints in terms of flight planning. The system used could only fly a maximum of 2 m AGL and was a one-dimensional system. Consequently, it was not suitable for use in larger-scale agriculture, and required cross-flying at a very low flying altitude compared to areas several hectares in size.

Overall, the potential of thermal imaging in agricultural applications warrants further investigation. To improve the accuracy of object identification in the field, it may be beneficial to collect image data over multiple days, increasing the likelihood of capturing optimal conditions.

4.5. Practical Implications and Implementation Outlook

Modern agricultural machinery is increasingly being equipped with standardized interfaces for geoinformation technologies—including for stone detection. The challenge here lies less in the technical feasibility than in the efficiency and practicality of data collection and processing. This study shows the potential of using thermal remote sensing for detecting surface stones, but emphasizes the high demands placed on sensor technology, flight planning, data processing and interpretation. Direct implementation by farmers,

especially on smaller farms, therefore seems unrealistic. Integration into existing services offered by contractors or remote sensing providers who already use UAV systems with RGB or multispectral sensors is more promising. Supplements using thermal imaging technology and automated analyses, e.g., stone maps or action-related recommendations, could be usefully embedded here. Specialist consultants could also play a central role in interpretation and operational implementation; for example, through targeted intervention strategies or cost–benefit analyses. The data obtained also offer potential for use in long-term management strategies, for example in soil protection or for optimizing the use of machinery. In this context, thermal stone detection should be seen as a modular component of digital agricultural systems. To promote its use, business models for UAV-based detection, integrated software solutions and training concepts for advisors should be developed in the future. The added value of the method ultimately results from its embedding in economically viable, user-friendly services that support decision-making at the farm level.

These reflections are based on the authors' experience from multi-year research and stakeholder engagement activities conducted within the AgriSens Demmin 4.0 project and its final workshops, which brought together perspectives from practitioners, advisors, technology providers, and researchers.

5. Conclusions

This study demonstrates that thermal remote sensing, when applied under suitable environmental conditions, holds significant potential for detecting surface stones in agricultural fields. By combining controlled laboratory experiments with UAV-based field data, it was shown that differential thermal inertia and emissivity enable reliable stone–soil separation—especially during periods of high soil moisture and declining ambient temperatures. Even minimal temperature contrasts proved sufficient for detection, underlining the sensitivity of thermal imaging in resolving thermophysical surface features.

This expands the established scope of UAV-based thermal applications, which include plant water stress detection, phenotyping, yield estimation [27], and archeological prospection [34], by introducing stone detection as a novel agricultural use case. Especially in low stone-density fields, thermal imaging combined with georeferenced data allows for targeted stone removal—reducing unnecessary soil compaction and operational effort compared to conventional mechanical methods, which remain better suited for high-density scenarios.

Compared to other remote sensing modalities, thermal imaging offers a unique advantage; while RGB and multispectral imaging rely on reflectance differences—which may be minimal in the case of dry stones on bare soil—and radar systems like SAR often lack the spatial resolution or surface sensitivity for small stone detection, thermal sensors directly measure physical heat signatures. This makes them especially effective for identifying thermally distinct features, independent of color, albedo, or microwave scattering behavior.

However, the study also highlights critical parameters for maximizing detection accuracy.

Sensor fusion potential: The integration of thermal data with multispectral or LiDAR sensors is expected to improve object discrimination and the spatial localization of stones. The authors have already carried out investigations into this, which go beyond the scope of this study. LiDAR, for example, provides high-resolution topography and object height data, which could help to distinguish stones from flat ground or vegetation artefacts. The data processing and development of evaluation algorithms is extremely complex. Similarly, multispectral indices can help to mask out vegetation or wet patches that interfere with thermal contrast.

Temporal optimization: The studies have shown the strong temporal effectiveness of thermal imaging. Data acquisition should be focused on times of maximum thermal

contrast. The results presented on the time-of-day strategies should be regarded as essential in future work processes and developed further.

Advanced data processing: The integration of image processing algorithms and machine learning methods can improve the reliability and scalability of stone detection. Techniques such as supervised classification, thermal anomaly detection or convolutional neural networks (CNN) offer promising possibilities for automatically distinguishing between stones and thermally similar objects (e.g., clods, debris). In research work currently underway, authors are analyzing this topic in detail, and a publication is in preparation.

Beyond agricultural applications, these findings open up possibilities in fields that require the detection of small, thermally distinct objects embedded in complex environments—ranging from wildlife conservation (e.g., locating ground-nesting birds) to cultural heritage detection or wildfire monitoring.

Future work should focus on cross-sensor data fusion frameworks, adaptive flight planning based on environmental parameters, and real-time onboard data processing to enable actionable outputs directly in the field. Thermal imaging, when thoughtfully integrated into a multi-sensor system, presents a scalable and cost-effective approach that aligns with the goals of precision agriculture and sustainable land use management.

Author Contributions: Conceptualization, F.T.; methodology, F.T.; validation, M.M. and F.T.; formal analysis, M.M. and F.T.; investigation, F.T.; resources, D.T., M.T. and F.T.; data curation, M.M. and F.T.; writing—original draft preparation, M.M.; writing—review and editing, F.T., M.M., D.T. and M.T.; visualization, M.M.; supervision, D.T., F.T. and M.T.; project administration, M.T., D.T. and F.T. All authors have read and agreed to the published version of the manuscript.

Funding: This research was funded by Bundesministerium für Ernährung und Landwirtschaft (BMEL); Federal Ministry of Food and Agriculture: 28DE114D18.

Data Availability Statement: The data presented in this study are available on request from the corresponding author. The data are not publicly available due to institutional data protection regulations.

Acknowledgments: The authors would like to thank the Laboratory "Geoökologisches Labor" of the Martin-Luther-University Halle-Wittenberg, Institute of Geosciences and Geography. During the preparation of this manuscript, the authors used ChatGPT-4o (OpenAI, accessed via https://chat.openai.com (accessed on 1 April 2025)) for the purposes of drafting and refining manuscript text, generating alternative title and keyword suggestions, and assisting in the development and troubleshooting of code for data analysis. The authors have reviewed and edited all AI-generated content and take full responsibility for the content of this publication.

Conflicts of Interest: Authors Florian Thürkow and Milena Mohri were employed by Umwelt-und Geodaten Management GbR. The remaining authors declare no conflicts of interest. The funders had no role in the design of the study; in the collection, analyses, or interpretation of data; in the writing of the manuscript; or in the decision to publish the results.

Appendix A

The appendix Figures A1–A5 display temperature differences (Stone–Soil vs. Stone–Soil Clod) to enable comparisons of thermal behavior between soil clods and soil.

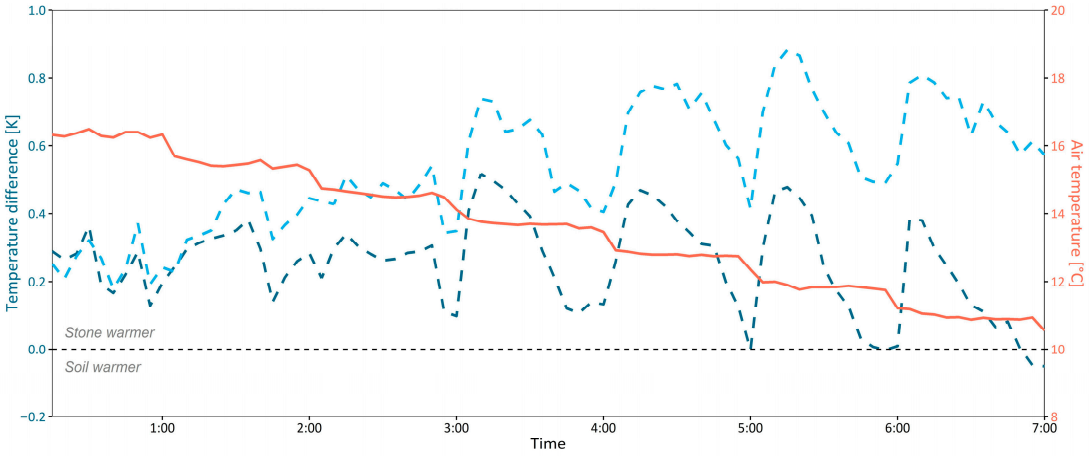

Figure A1. Temperature differences between the stones and the soil (darkblue) and stones and soil clods (lightblue) for dry soil conditions measured by the thermal camera and surrounding air temperature (red).

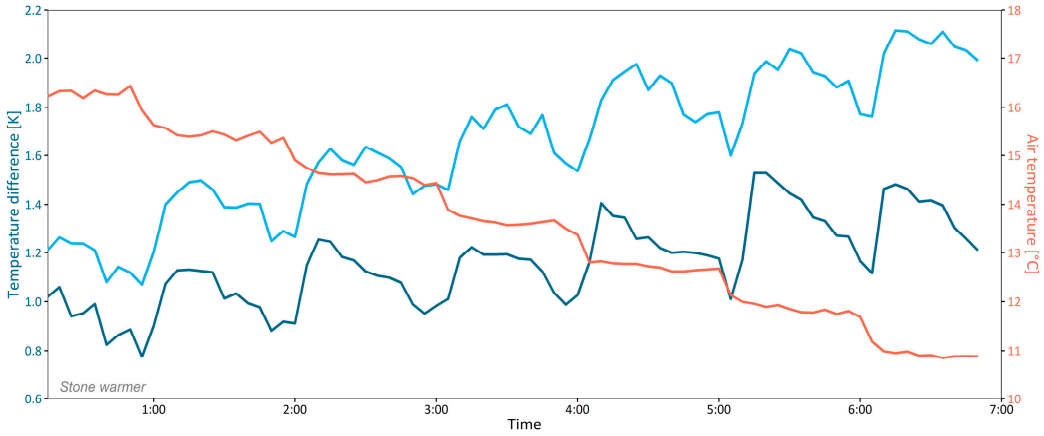

Figure A2. Temperature differences between the stones and the soil (darkblue) and stones and soil clods (lightblue) for moist soil conditions measured by the thermal camera and surrounding air temperature (red).

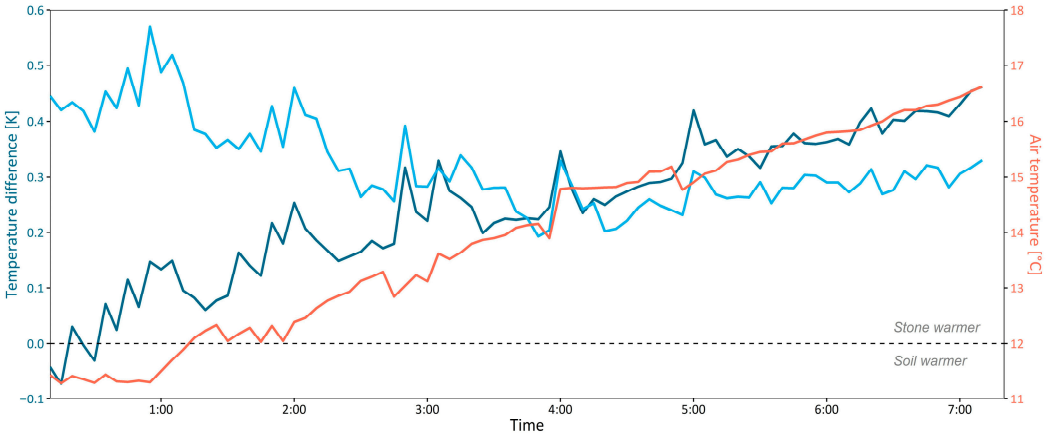

Figure A3. Temperature differences between the stones and the soil (darkblue) and stones and soil clods (lightblue) for moist soil conditions measured by the thermal camera and surrounding air temperature (red).

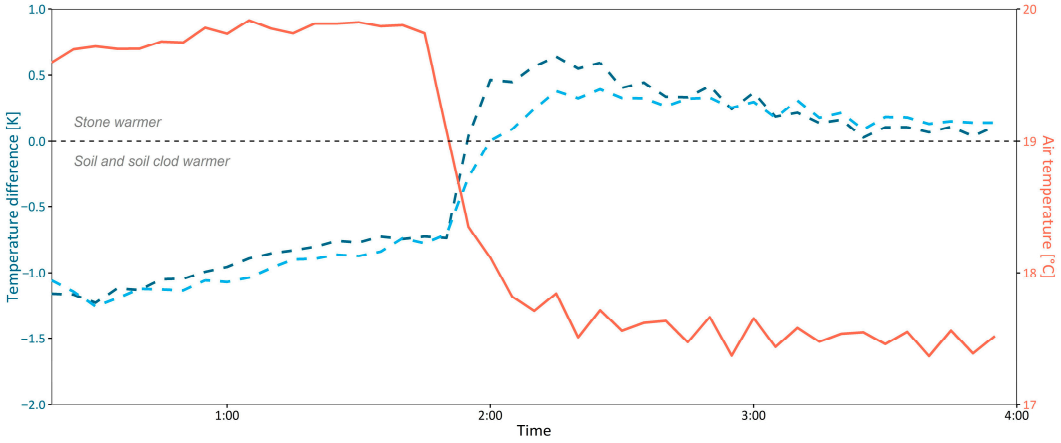

Figure A4. Temperature differences between the stones and the soil (darkblue) and stones and soil clods (lightblue) for dry soil conditions measured by the thermal camera and surrounding air temperature (red).

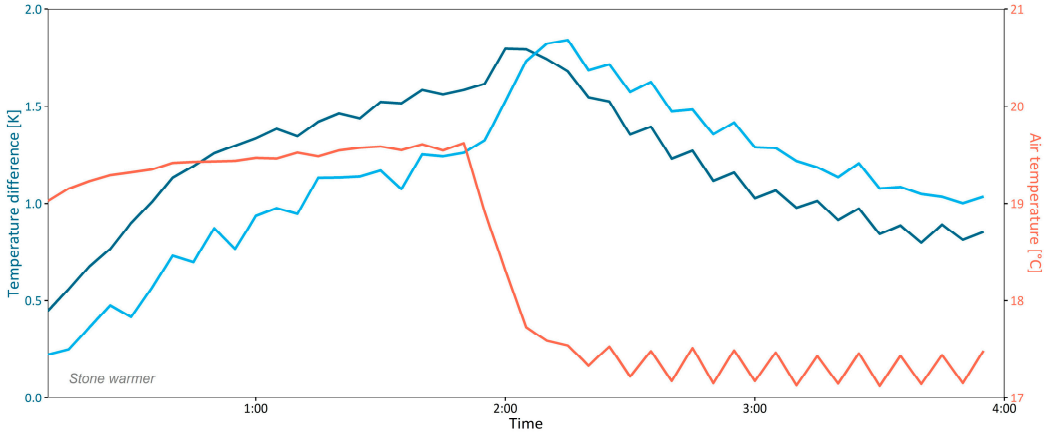

Figure A5. Temperature differences between the stones and the soil (darkblue) and stones and soil clods (lightblue) for moist soil conditions measured by the thermal camera and surrounding air temperature (red).

References

1. Toscano, P.; Brambilla, M.; Cutini, M.; Bisaglia, C. The Stony Soils Reclamation Systems in Agricultural Lands: A Review. *Agric. Sci.* **2022**, *13*, 500–519. [CrossRef]
2. Dexter, A.R. Soil Physical Quality. *Geoderma* **2004**, *120*, 201–214. [CrossRef]
3. Kirchner, A.; Rakitsch, S.; Benning, R.; Günthner, W.A. *Fremdstoffe in Agrarrohstoffen—Charakteristik Und Bewertung Des Schadenspotenzials Bei Der Stetigförderung in Umschlagsanlagen*; fml—Lehrstuhl für Fördertechnik Materialfluss Logistik; Technische Universität München: Garching, Germany, 2013.
4. Rakitsch, S.; Günthner, W.A.; Kirchner, A.; Feil, A. Schadenspotential von Fremdstoffen in Agrarrohstoffen. In Proceedings of the 16. Fachtagung Schüttgutfördertechnik 2011: Anlagen—Bauteile—Computersimulationen; Technische Universität München: München, Germany, 2011; pp. 188–195.
5. Gage, J.E.; Gage, M.E. Field Clearing: Stone Removal and Disposal Practices in Agriculture & Farming. *Crops* **2014**, *213*, 6–29.
6. Rytter, R.-M. Stone and Gravel Contents of Arable Soils Influence Estimates of C and N Stocks. *Catena* **2012**, *95*, 153–159. [CrossRef]
7. Ballabio, C.; Panagos, P.; Monatanarella, L. Mapping Topsoil Physical Properties at European Scale Using the LUCAS Database. *Geoderma* **2016**, *261*, 110–123. [CrossRef]
8. Toscano, P.; Cutini, M.; Cabassi, G.; Pricca, N.; Romano, E.; Bisaglia, C. Assessment of a Deep Burial Destoning System of Agrarian Soils Alternative to the Stone Removal and On-Site Crushing. *AgriEngineering* **2022**, *4*, 156–170. [CrossRef]
9. Biryan, H.; Yilmaz, A.M. Stoniness and Erosion Problems in Cultivated Lands of Konya Province (Turkey) and Solution Suggestions. *Int. J. Ecosyst. Ecol. Sci.* **2012**, *2*, 21–26.
10. Baganz, K. Die Maschinelle Steinentfernung Im Norddeutschen Moränengebiet. *Agrartechnik.* **1962**, *2*, 62–68.

11. Steine Sammeln Mit Der Maschine. Unser Land 2019. Available online: https://www.youtube.com/watch?v=9CuQrywKAUI&pp=0gcJCfcAhR29_xXO (accessed on 20 March 2025).
12. Hunger, R. Marktübersicht—Steinsammler: Ergänzung Zum Schwerpunkt «Mechanische Unkrautregulierung». 2019. Available online: https://www.agrartechnik.ch/fileadmin/user_upload/downloads_de/SP_Homepage_Hunger_Steinsammler.pdf (accessed on 25 March 2025).
13. Altmann GmbH Kivi-Pekka 5m Steinsammler—Produktinformation 2017. Available online: https://www.altmann-gmbh.at/images/werbung/2017-09-01NewsletterMaschinenangebote/addon/KiviPeka.pdf (accessed on 26 March 2025).
14. Lacy, K.; Whitt, C.; Lim, K. Most Small Family Farms Are at High Financial Risk Based on Operating Profit Margin 2022. Available online: https://www.ers.usda.gov/data-products/charts-of-note/chart-detail?chartId=108317 (accessed on 30 March 2025).
15. Bhakta, I.; Phadikar, S.; Majumder, K. State-of-the-art Technologies in Precision Agriculture: A Systematic Review. *J. Sci. Food Agric.* **2019**, *99*, 4878–4888. [CrossRef]
16. Nowak, B. Precision Agriculture: Where Do We Stand? A Review of the Adoption of Precision Agriculture Technologies on Field Crops Farms in Developed Countries. *Agric. Res.* **2021**, *10*, 515–522. [CrossRef]
17. Monteiro, A.; Santos, S.; Gonçalves, P. Precision Agriculture for Crop and Livestock Farming—Brief Review. *Animals* **2021**, *11*, 2345. [CrossRef] [PubMed]
18. Aby, G.R.; Issa, S.F. Safety of Automated Agricultural Machineries: A Systematic Literature Review. *Safety* **2023**, *9*, 13. [CrossRef]
19. Mukhamediev, R.I.; Symagulov, A.; Kuchin, Y.; Zaitseva, E.; Bekbotayeva, A.; Yakunin, K.; Assanov, I.; Levashenko, V.; Popova, Y.; Akzhalova, A.; et al. Review of Some Applications of Unmanned Aerial Vehicles Technology in the Resource-Rich Country. *Appl. Sci.* **2021**, *11*, 10171. [CrossRef]
20. Tyagi, R.; Pandey, P.C. Applications of Drones in Precision Agriculture: Future of Smart and Sustainable Farming. In *Remote Sensing in Precision Agriculture*; Elsevier: Amsterdam, The Netherlands, 2024; pp. 429–453. ISBN 978-0-323-91068-2.
21. Olson, D.; Anderson, J. Review on Unmanned Aerial Vehicles, Remote Sensors, Imagery Processing, and Their Applications in Agriculture. *Agron. J.* **2021**, *113*, 971–992. [CrossRef]
22. Tsouros, D.C.; Bibi, S.; Sarigiannidis, P.G. A Review on UAV-Based Applications for Precision Agriculture. *Information* **2019**, *10*, 349. [CrossRef]
23. Sishodia, R.P.; Ray, R.L.; Singh, S.K. Applications of Remote Sensing in Precision Agriculture: A Review. *Remote Sens.* **2020**, *12*, 3136. [CrossRef]
24. Zhang, Z.; Zhu, L. A Review on Unmanned Aerial Vehicle Remote Sensing: Platforms, Sensors, Data Processing Methods, and Applications. *Drones* **2023**, *7*, 398. [CrossRef]
25. Huo, D.; Malik, A.W.; Ravana, S.D.; Rahman, A.U.; Ahmedy, I. Mapping Smart Farming: Addressing Agricultural Challenges in Data-Driven Era. *Renew. Sustain. Energy Rev.* **2024**, *189*, 113858. [CrossRef]
26. Hassler, S.C.; Baysal-Gurel, F. Unmanned Aircraft System (UAS) Technology and Applications in Agriculture. *Agronomy* **2019**, *9*, 618. [CrossRef]
27. Messina, G.; Modica, G. Applications of UAV Thermal Imagery in Precision Agriculture: State of the Art and Future Research Outlook. *Remote Sens.* **2020**, *12*, 1491. [CrossRef]
28. Wilson, A.N.; Gupta, K.A.; Koduru, B.H.; Kumar, A.; Jha, A.; Cenkeramaddi, L.R. Recent Advances in Thermal Imaging and Its Applications Using Machine Learning: A Review. *IEEE Sens. J.* **2023**, *23*, 3395–3407. [CrossRef]
29. Badgujar, C.M.; Poulose, A.; Gan, H. Agricultural Object Detection with You Only Look Once (YOLO) Algorithm: A Bibliometric and Systematic Literature Review. *Comput. Electron. Agric.* **2024**, *223*, 109090. [CrossRef]
30. Ariza-Sentís, M.; Vélez, S.; Martínez-Peña, R.; Baja, H.; Valente, J. Object Detection and Tracking in Precision Farming: A Systematic Review. *Comput. Electron. Agric.* **2024**, *219*, 108757. [CrossRef]
31. Awais, M.; Li, W.; Cheema, M.J.M.; Zaman, Q.U.; Shaheen, A.; Aslam, B.; Zhu, W.; Ajmal, M.; Faheem, M.; Hussain, S.; et al. UAV-Based Remote Sensing in Plant Stress Imagine Using High-Resolution Thermal Sensor for Digital Agriculture Practices: A Meta-Review. *Int. J. Environ. Sci. Technol.* **2023**, *20*, 1135–1152. [CrossRef]
32. Das, S.; Chapman, S.; Christopher, J.; Choudhury, M.R.; Menzies, N.W.; Apan, A.; Dang, Y.P. UAV-Thermal Imaging: A Technological Breakthrough for Monitoring and Quantifying Crop Abiotic Stress to Help Sustain Productivity on Sodic Soils—A Case Review on Wheat. *Remote Sens. Appl. Soc. Environ.* **2021**, *23*, 100583. [CrossRef]
33. Ishimwe, R.; Abutaleb, K.; Ahmed, F. Applications of Thermal Imaging in Agriculture—A Review. *Adv. Remote Sens.* **2014**, *3*, 128–140. [CrossRef]
34. Casana, J.; Wiewel, A.; Cool, A.; Hill, A.C.; Fisher, K.D.; Laugier, E.J. Archaeological Aerial Thermography in Theory and Practice. *Adv. Archaeol. Pract.* **2017**, *5*, 310–327. [CrossRef]
35. Nikiforova, T.; Savytskyi, M.; Limam, K.; Bosschaerts, W.; Belarbi, R. Methods and Results of Experimental Researches of Thermal Conductivity of Soils. *Energy Procedia* **2013**, *42*, 775–783. [CrossRef]
36. Robertson, E.C. *Thermal Properties of Rocks*; US Geological Survey: Reston, VA, USA, 1988.

37. Reiniger, P.; Seguin, B. Surface Temperature as an Indicator of Evapotranspiration and Soil Moisture. *Remote Sens. Rev.* **1986**, *1*, 277–310. [CrossRef]
38. Schmer, F.A.; Werner, H.D. Remote Sensing Techniques for Evaluation of Soil Water Conditions. *Trans. ASAE* **1974**, *17*, 310–314. [CrossRef]
39. Minacapilli, M.; Cammalleri, C.; Ciraolo, G.; D'Asaro, F.; Iovino, M.; Maltese, A. Thermal Inertia Modeling for Soil Surface Water Content Estimation: A Laboratory Experiment. *Soil Sci. Soc. Am. J.* **2012**, *76*, 92–100. [CrossRef]
40. Deutscher Wetterdienst (DWD) Historical Daily Climate Data (KL)—Station Observations for Greifswald (ID: 01757) and Anklam (ID: 00167) 2025. Available online: https://opendata.dwd.de/climate_environment/CDC/observations_germany/climate/ (accessed on 1 March 2025).
41. ThermoWorks ThermoWorks—Infrared Emissivity Table. Available online: https://www.thermoworks.com/emissivity-table/ (accessed on 18 March 2025).
42. DJI Innovations DJI Thermal SDK, v1.6; 2024. Available online: https://www.dji.com/it/downloads/softwares/dji-thermal-sdk (accessed on 15 February 2025).
43. RStudio Team. RStudio: Integrated Development Environment for R; 2024. Available online: https://posit.co/download/rstudio-desktop/ (accessed on 2 February 2025).
44. R Core Team. *R: A Language and Environment for Statistical Computing*; Version 4.4.2; R Foundation for Statistical Computing: Vienna, Austria, 2024; Available online: https://cran.r-project.org/bin/windows/base/old/ (accessed on 2 February 2025).
45. Grolemund, G.; Wickham, H. Dates and Times Made Easy with Lubridate. *J. Stat. Softw.* **2011**, *40*, 1–25. [CrossRef]
46. Urbanek, S.; Johnson, K. Tiff: Read and Write TIFF Images; 2023. Available online: https://CRAN.R-project.org/package=tiff (accessed on 2 February 2025).
47. Thoen, E. Padr: Quickly Get Datetime Data Ready for Analysis; 2024. Available online: https://CRAN.R-project.org/package=padr (accessed on 2 February 2025).
48. Chang, W. Extrafont: Tools for Using Fonts; 2023. Available online: https://CRAN.R-project.org/package=extrafont (accessed on 2 February 2025).
49. Wickham, H. *Ggplot2: Elegant Graphics for Data Analysis*; Springer: New York, NY, USA, 2016; ISBN 978-3-319-24277-4.
50. Wickham, H.; François, R.; Henry, L.; Müller, K.; Vaughan, D. Dplyr: A Grammar of Data Manipulation; 2023. Available online: https://CRAN.R-project.org/package=dplyr (accessed on 2 February 2025).
51. Kuenzer, C.; Dech, S. Theoretical Background of Thermal Infrared Remote Sensing. In *Thermal Infrared Remote Sensing: Sensors, Methods, Applications*; Springer: Dordrecht, The Netherlands, 2013; Volume 17, pp. 1–26.
52. Waples, D.W.; Waples, J.S. A Review and Evaluation of Specific Heat Capacities of Rocks, Minerals, and Subsurface Fluids. Part 1: Minerals and Nonporous Rocks. *Nat. Resour. Res.* **2004**, *13*, 97–122. [CrossRef]
53. Wang, Y.; Lu, Y.; Horton, R.; Ren, T. Specific Heat Capacity of Soil Solids: Influences of Clay Content, Organic Matter, and Tightly Bound Water. *Soil Sci. Soc. Am. J.* **2019**, *83*, 1062–1066. [CrossRef]
54. Sundberg, J. Thermal Properties of Soils and Rocks. 1988. Available online: https://www.researchgate.net/profile/Jan-Sundberg-4/publication/35391832_Thermal_properties_of_soils_and_rocks/links/5621216e08ae93a5c927da59/Thermal-properties-of-soils-and-rocks.pdf (accessed on 24 March 2025).
55. Jia, R.; Liu, J.; Zhang, J.; Niu, Y.; Jiang, Y.; Xuan, K.; Wang, C.; Ji, J.; Ma, B.; Li, X. An Improved UAV-Based ATI Method Incorporating Solar Radiation for Farm-Scale Bare Soil Moisture Measurement. *Remote Sens.* **2023**, *15*, 3769. [CrossRef]
56. Civeira, G. *Soil Moisture*; Civeira, G., Ed.; IntechOpen: London, UK, 2019; ISBN 978-1-78985-103-8.
57. Pratt, D.A.; Ellyett, C.D. The Thermal Inertia Approach to Mapping of Soil Moisture and Geology. *Remote Sens. Environ.* **1979**, *8*, 151–168. [CrossRef]
58. Waagen, J.; Sánchez, J.G.; Van Der Heiden, M.; Kuiters, A.; Lulof, P. In the Heat of the Night: Comparative Assessment of Drone Thermography at the Archaeological Sites of Acquarossa, Italy, and Siegerswoude, The Netherlands. *Drones* **2022**, *6*, 165. [CrossRef]
59. Sun, L.; Sun, R.; Li, X.; Liang, S.; Zhang, R. Monitoring Surface Soil Moisture Status Based on Remotely Sensed Surface Temperature and Vegetation Index Information. *Agric. For. Meteorol.* **2012**, *166–167*, 175–187. [CrossRef]
60. Hillel, D. *Environmental Soil Physics*; Academic Press: San Diego, CA, USA; London, UK; Boston, MA, USA; New York, NY, USA; Sydney, Australia; Tokyo, Japan; Toronto, ON, Canada; p. 329. ISBN 978-0-12-348525-0.
61. Sayão, V.M.; Demattê, J.A.M.; Bedin, L.G.; Nanni, M.R.; Rizzo, R. Satellite Land Surface Temperature and Reflectance Related with Soil Attributes. *Geoderma* **2018**, *325*, 125–140. [CrossRef]
62. Wang, L.; Qu, J.J. Satellite Remote Sensing Applications for Surface Soil Moisture Monitoring: A Review. *Front. Earth Sci. China* **2009**, *3*, 237–247. [CrossRef]
63. Zhang, D.; Zhou, G. Estimation of Soil Moisture from Optical and Thermal Remote Sensing: A Review. *Sensors* **2016**, *16*, 1308. [CrossRef] [PubMed]

64. Holzman, M.E.; Rivas, R.; Piccolo, M.C. Estimating Soil Moisture and the Relationship with Crop Yield Using Surface Temperature and Vegetation Index. *Int. J. Appl. Earth Obs. Geoinf.* **2014**, *28*, 181–192. [CrossRef]
65. Lu, S.; Ju, Z.; Ren, T.; Horton, R. A General Approach to Estimate Soil Water Content from Thermal Inertia. *Agric. For. Meteorol.* **2009**, *149*, 1693–1698. [CrossRef]
66. Cheruy, F.; Dufresne, J.L.; Aït Mesbah, S.; Grandpeix, J.Y.; Wang, F. Role of Soil Thermal Inertia in Surface Temperature and Soil Moisture-Temperature Feedback. *J. Adv. Model Earth Syst.* **2017**, *9*, 2906–2919. [CrossRef]
67. Bosse, O.; Forbriger, U.; Hanisch, J. Neue Werkzeuge Für Findlingsrodung Und Tieflockerung. *Agrartechnik* **1977**, *7*, 320–321.